Spinon Heat Transport in the Three-Dimensional Quantum Magnet $PbCuTe_2O_6$

Xiaochen Hong,[1,2] Matthias Gillig,[2] Abanoub R. N. Hanna,[3,4] Shravani Chillal,[4] A. T. M. Nazmul Islam,[4] Bella Lake,[3,4] Bernd Büchner,[2,5] and Christian Hess[1,2,*]

[1]*Fakultät für Mathematik und Naturwissenschaften, Bergische Universität Wuppertal, Gaußstraße 20, 42119 Wuppertal, Germany*
[2]*Leibniz-Institute for Solid State and Materials Research (IFW-Dresden), Helmholtzstraße 20, 01069 Dresden, Germany*
[3]*Institut für Festkörperforschung, Technische Universität Berlin, Hardenbergstraße 36, 10623 Berlin, Germany*
[4]*Helmholtz-Zentrum Berlin für Materialien und Energie, Hahn-Meitner Platz 1, 14109 Berlin, Germany*
[5]*Institute of Solid State and Materials Physics and Würzburg-Dresden Cluster of Excellence ct.qmat, Technische Universität Dresden, 01062 Dresden, Germany*

(Received 19 July 2023; accepted 15 November 2023; published 18 December 2023)

Quantum spin liquids (QSLs) are novel phases of matter which remain quantum disordered even at the lowest temperature. They are characterized by emergent gauge fields and fractionalized quasiparticles. Here we show that the sub-kelvin thermal transport of the three-dimensional $S = 1/2$ hyperhyperkagome quantum magnet $PbCuTe_2O_6$ is governed by a sizeable charge-neutral fermionic contribution which is compatible with the itinerant fractionalized excitations of a spinon Fermi surface. We demonstrate that this hallmark feature of the QSL state is remarkably robust against sample crystallinity, large magnetic field, and field-induced magnetic order, ruling out the imitation of QSL features by extrinsic effects. Our findings thus reveal the characteristic low-energy features of $PbCuTe_2O_6$ which qualify this compound as a true QSL material.

DOI: 10.1103/PhysRevLett.131.256701

Quantum spin liquid (QSL) states refer to highly entangled magnetic quantum ground states realized in frustrated magnets [1,2]. Despite the quantum disorder of the ground states, the QSLs possess well-defined emergent fractionalized excitations such as spinons, Majorana fermions, visons, and many more [1–6], rendering them tantalizing since their initial proposal [7]. Recent years have witnessed the progress of materializing the QSL models [8], which has stimulated intense interest from both experimental and theoretical sides [3,4]. By far, most efforts in this field are devoted to two-dimensional systems because enhanced quantum fluctuations, an ingredient for realizing QSL states, are prominent in reduced dimensionality [2–4]. Nevertheless, there are also some three-dimensional (3D) QSL candidates. The most prominent model systems are examples of pyrochlore, hyperkagome, and double-layer kagome lattices [9–13].

Among the handful of candidate QSL materials, clear-cut evidence for the anticipated emergent fractionalized magnetic excitations, in particular, the spinons, is rather scarce [3,4]. Thermal conductivity, a probe only sensitive to itinerant entropy carriers, is the method of choice to prove the existence of spinons via their fermionic nature and their mobility [14,15]. These important pieces of information are difficult to diagnose by thermodynamic or spectroscopic studies. To be specific, the spinon contribution to the heat conductivity κ_{spinon} is expected to be linear in temperature (T) toward $T \to 0$ K [15], reminiscent of the electronic κ_e in metals. Except for some one-dimensional spin-chain systems [16–18], compelling experimental evidence for this sought-after κ_{spinon} signaling a spinon Fermi surface is still pending. Earlier reports for κ_{spinon} in other QSL candidate materials have been shown to suffer from irreproducibility [19–23]. Some other QSL-like results can actually be explained by a peculiar phononic background resulting from spin scattering [24–27]. It is also argued that defects and impurities in a genuine QSL material can easily eliminate its fingerprints in thermal transport [23,28,29], preventing a reconciliation with other experimental techniques with which disorders do just the opposite, producing fraudulent QSL-like results in trivial systems [30–32]. It is therefore essential to exclude all these problems in order to reveal true evidence for fermionic spinon heat transport, κ_{spinon}.

Choloalite $PbCuTe_2O_6$ crystallizes into a cubic $P4_132$ structure at ambient temperature [33,34]. Its magnetic Cu^{2+} ions ($S = 1/2$) constitute a 3D network similar to the Ir^{4+} ions in the hyperkagome material $Na_4Ir_3O_8$ [10]. However, density functional theory calculations of $PbCuTe_2O_6$ suggest its nearest neighbor ($J_1 = 1.13$ meV, giving isolated triangles) and next-nearest neighbor ($J_2 = 1.07$ meV, giving a hyperkagome lattice) interactions are almost of the same strength [35]. As a result, each Cu^{2+} ion is at the corner of three triangles rather than two triangles as for the hyperkagome case. The Cu^{2+} lattice of $PbCuTe_2O_6$ thus possesses four-site and six-site loops as its shortest spin rings [35], distinct from the ten-site loop of a standard

hyperkagome lattice [36,37], and was referred to as hyper-hyperkagome lattice [35]. An antiferromagnetic Curie-Weiss temperature $\Theta_{CW} \approx -22$ K was inferred from the magnetic susceptibility data of $PbCuTe_2O_6$ [34], but no magnetic order has been found down to 20 mK (frustration parameter $f = |\Theta_{CW}/T_N| > 1000$, where T_N is the Néel temperature) [34,35,38]. $PbCuTe_2O_6$ possesses a ferroelectric (FE) transition at around 1 K, accompanied by a structural transition to a lower symmetry phase [39,40]. Notably, both the FE and structural distortions are absent in small-grained polycrystalline samples [39]. Regardless of this difference, characteristic multispinon continua of the magnetic excitations were identified by inelastic neutron scattering in both polycrystalline and single crystalline $PbCuTe_2O_6$ samples [35], down to 100 mK (below T_{FE}). This places $PbCuTe_2O_6$ on the short list of promising QSL materials with emergent spinon excitations.

In this Letter, we report clear evidence of spinon heat transport in this 3D QSL candidate material $PbCuTe_2O_6$ at very low temperature, revealed by a sizeable T-linear contribution (κ_{spinon}) to the total thermal conductivity κ, which adds to the well-known T^3 contribution of phonons (κ_{ph}) [41]. Three different batches of $PbCuTe_2O_6$ samples prepared by different techniques, namely, two differently fabricated single crystals and one polycrystalline sample, were involved in this study [42]. κ of all samples has been studied at $T < 1$ K as well as at 6 K $\leq T \leq$ 160 K [42]. Despite a rich H-T phase diagram of $PbCuTe_2O_6$, the signature of spinon heat transport is robust in all samples across the investigated parameter range.

As presented in Fig. 1(a), the low-T $\kappa(T)$ of the single crystalline sample S1 at zero field shows distinct fingerprints of a spinon Fermi surface, i.e., a linear contribution to κ. This can easily be seen from the figure which shows the measured κ/T versus T^2. In this representation, the linear contribution on top of a standard phononic background ($\kappa_{ph} \propto T^3$ [53]) is just the residual at 0 K [15]. Indeed, above a certain $T_{drop} \approx 340$ mK, the data can be well fitted according to $\kappa/T = a + b \times T^2$. Here, $bT^2 \equiv \kappa_{ph}/T$ yields the expected phononic background with $b = 0.206$ mW/(K^4 cm) [54]. The residual $a = 0.075$ mW/(K^2 cm), as indicated by the red dot, represents a fermionic contribution to the heat conductivity. For insulating magnets such as $PbCuTe_2O_6$, such a fermionic contribution can only be explained by pertinent fractionalized magnetic excitations [14,19]. The data thus provide clear-cut evidence for a spinon contribution, $\kappa_{spinon} \equiv aT$.

Our above conclusion of spinon heat transport and its quantitative determination is corroborated by our measurements of κ/T in magnetic fields. Figure 1(b) shows $\kappa/T(T)$ of sample S1 in magnetic fields up to $\mu_0 H = 16$ T, with the field applied perpendicular to the heat current. The curves are only slightly affected by the field up to $\mu_0 H = 10$ T, and are shifted up with a nearly unaltered bT^2 term at higher

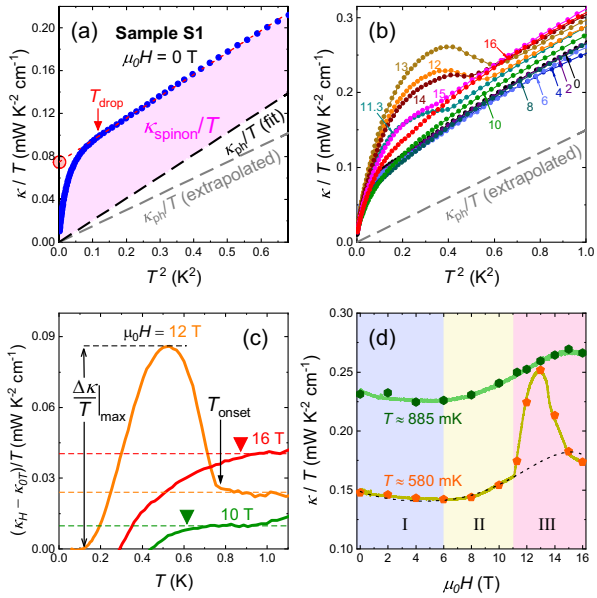

FIG. 1. (a) κ/T versus T^2 of sample S1 in zero field, and extraction of κ_{ph} and κ_{spinon}; see text. The red dotted line represents a linear fit to κ/T above T_{drop} (red arrow), and its extrapolation to $T = 0$, yielding the linear residual $a \equiv \kappa_{spinon}/T$ (red dot). The dashed black line represents the thus extracted κ_{ph}/T. The spinon contribution κ_{spinon}/T on top of κ_{ph}/T is highlighted as the magenta region. The dashed gray line represents the extrapolated κ_{ph}/T from the $\kappa(T)$ data above 6 K [42,54]. (b) $\kappa/T(T^2)$ in field together with the same extrapolated κ_{ph}/T curve as in panel (a). (c) Field effect on κ for three representative field values after subtracting the zero field value $(\kappa_H - \kappa_{0T})/T$. T_{drop} is highlighted by triangles, and the definition of the peak height ($(\Delta\kappa/T)|_{max}$) is exemplified. (d) Field dependence of κ/T isotherms measured at two selected temperatures (thick solid lines) plotted with the results (full symbols) extracted from the fixed-field $\kappa(T)/T$ data. Three different regions can be identified and are displayed by the different background colors. The black dashed line represents the higher-temperature isotherm (green band) subtracted by a fixed value of 0.085 mW/(K^2 cm); see text.

fields. This renders our data fundamentally different from recently claimed evidence for a spinon residual κ_{spinon}/T term in several QSL candidate materials [24–26], where a large magnetic field leads to a strong enhancement (factor $2, \ldots, 10$) of κ and bT^2 [27,55,56]. Contrastingly, the practically field-independent bT^2 term in $PbCuTe_2O_6$ and the fact that the pure $\kappa_{ph}/T(T)$ curve is well below the total $\kappa/T(T)$ curves leave no room for a phononic-only explanation to the residual a as found in other frustrated magnets [27], confirming the κ_{spinon} transport channel.

We point out that while κ_{ph} remains weakly affected by the magnetic field, it still has a clear impact on the total κ. First, as represented by the 12 T curve in Fig. 1(c) and also visible directly in Fig. 1(b), an additional $\kappa/T(T)$ peak on top of the phonon and spinon contributions emerges below T_{onset} in the field range of 11 T $< \mu_0 H <$ 15 T. Both the

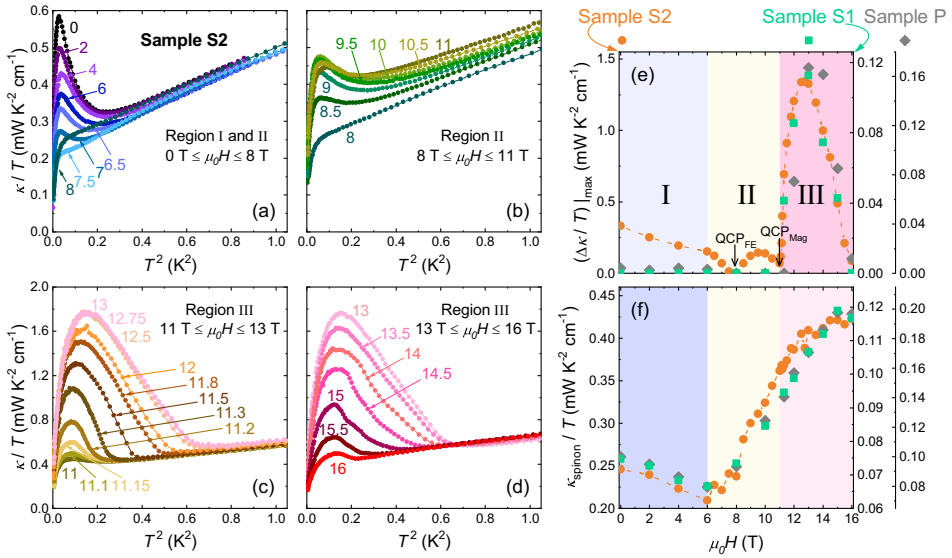

FIG. 2. The $\kappa/T(T^2)$ curves of sample S2 separated into four panels (a)–(d) for clarity. The field dependence of the extracted amplitude of (e) the peaks and (f) the residual linear term κ_0/T are compared among all samples. The ferroelectric (QCP_{FE}) and magnetic (QCP_{mag}) critical points [57] are marked by the black arrows. Note the distinct ordinates with different scales. The determination of field regions is inherited from Fig. 1(d).

T_{onset} and the amplitude of the new peak are highly field sensitive. Eventually, at $\mu_0 H = 16$ T the peak is absent again, and the low field behavior of $\kappa/T(T)$ is recovered with a rather higher value of $T_{drop} \approx 870$ mK. Second, T_{drop}, which apparently represents an energy scale above which κ_{spinon} can be observed, increases with the field. As an example shown in Fig. 1(c), $T_{drop} \approx 610$ mK at $\mu_0 H = 10$ T. Finally, the residual $a \equiv \kappa_{spinon}/T$ increases considerably in this high field region above 10 T.

The general field evolution of κ/T is more clearly presented in Fig. 1(d) as $\kappa/T(H)$ isotherms. The high-T (885 mK, above T_{onset}) isotherm shows a minor decrease at small fields, followed by a slight continuous increase of κ/T above $\mu_0 H \approx 6$ T, until its saturation around $\mu_0 H = 15$ T. This increment is entirely due to κ_{spinon}, as was discussed above. On the other hand, the lower-T (580 mK, below T_{onset}) isotherm is more complicated, featuring a large hump centered at 13 T. Three field regions can thus be discerned based on the isotherms. The $\kappa/T(H)$ isotherms first decrease mildly in region I, and then increase somewhat faster in region II. Region III is defined by the occurrence of the peak. It is worthwhile to point out that the two isotherms match nicely in regions I and II through shifting by a constant value of 0.085 mW/(K^2 cm), i.e., the difference in the phononic contribution $b \times [(0.885\ \mathrm{K})^2 - (0.58\ \mathrm{K})^2]$. This fact strongly suggests that a new contributor to κ comes into play below T_{onset} in region III, which will be discussed further below.

In order to evaluate whether any of the observed heat transport phenomenology described above is affected by the ferroelectric and accompanying structural transitions at $T_{FE} \approx 1$ K, we performed another heat transport measurement on a sample lacking the FE transition, namely, the unannealed polycrystalline sample P. With regard to the heat transport, it behaves basically the same as the single crystalline sample S1 in the same T and H parameter range [42]. Thus, our above observations represent the intrinsic phenomenology of $PbCuTe_2O_6$, which is apparently independent of the ferroelectric or structural transitions. Note that our $\kappa/T(T)$ curves show no anomaly at around 1 K [42], in contrast to the specific heat, which underpins this statement [39,40,57,58]. This finding is important, because it demonstrates that the inferred κ_{spinon} is unaffected by the symmetry reduction induced by the ferroelectric order and the accompanying structural phase transition. Hence, our conclusion of compatibility with a QSL ground state remains robust even if the subtle noncubic distortion present in the single crystalline sample S1 below 1 K is taken into account [40].

After having established the intrinsic low-temperature heat transport behavior of $PbCuTe_2O_6$, we turn now to the single crystalline sample S2 which (unlike the phase-pure samples sample S1 and sample P [42]) is known to contain a small amount of nonmagnetic $Pb_2Te_3O_8$ inclusions in an otherwise phase pure $PbCuTe_2O_6$ matrix [35,39]. The most obvious difference of the $\kappa(T)/T$ curves of sample S2 shown in Figs. 2(a)–2(d) compared to samples S1 and P is an additional $\kappa/T(T)$ peak below $\mu_0 H = 11$ T (in regions I and II). It is highly sensitive to H, as embodied more clearly in Fig. 2(e), where the extracted peak height of sample S2 reveals a sharp dip at $\mu_0 H \approx 8$ T, exactly the field at which the ferroelectric transition is driven to its critical point ($H_{QCP(FE)} = 7.9$ T) [57]. On the other hand, it is insensitive

to the boundary between region I and region II. At higher field, the additional peak is preempted by the feature bounded to region III. Although the $\kappa/T(T)$ peak of sample S2 in region III is much more pronounced as compared to samples S1 and P, their extracted contributions ($\Delta\kappa/T|_{\mathrm{max}}$) match extremely well after normalizing the peaks by their maximum value at 13 T [see Fig. 2(e)]. The field-dependent spinon contribution $\kappa_{\mathrm{spinon}}/T$ is also extracted from the dataset above T_{onset}, and compared among all three samples, as presented in Fig. 2(f). Again, they fit very well modulo a proper rescaling factor. In all samples, the $\kappa_{\mathrm{spinon}}/T$ values at 16 T increase by 70% or more with respect to their 0 T values. Further theoretical investigations are required to rationalize this field dependence. At present, one may speculate that it results from a field-induced variation of the spinon band width [59], or a field-induced shift of the spinon chemical potential [60].

It is very revealing to plot our main findings together with a recently established thermodynamic T-H phase diagram of the ferroelectric (T_{FE}), magnetic (T_{M}), and structural (T_{S}) orders at low T [57]; see Fig. 3. Clearly, the onsets of the additional $\kappa/T(T)$ peak in region III ($\mu_0 H > 11$ T) match the thermodynamic magnetic ordering temperatures T_{M} [57]. Hence, the excess heat conductivity which causes the peak can unambiguously be attributed to magnon transport. Note that magnons obey a bosonic behavior and emerge from long-range magnetic order in contrast to the spinons. At lower fields, the presence of the excess $\kappa/T(T)$ peak is obviously sample dependent since it can only be resolved for sample S2. Here, the onset temperature (T_{onset}) and the peak height [see Fig. 2(e)] track at $H < H_{\mathrm{QCP(FE)}}$ the ferroelectric order (T_{FE}) at somewhat lower T and recover at $H_{\mathrm{QCP(FE)}} < H < 11$ T in the structurally distorted phase. It is therefore closely connected with the symmetry reduction due to the ferroelectric order and/or the structural distortion. Since phonons clearly are not sensitive to this symmetry reduction (see above), this low-T peak must be of magnetic origin. Despite the fact that magnetic order could not be detected below 11 T in previous works [34,35,38–40,57], we therefore assign also this peak to magnon transport. It is known that $PbCuTe_2O_6$ is proximate to magnetic order [38,40], and our data indicate that the disordered crystal matrix in sample S2 due to the $Pb_2Te_3O_8$ inclusions drives this sample to magnetic order at low T. Overall, the most exotic finding of this work, the spinon contribution to thermal transport, prevails throughout the phase diagram until it is either freezing below T_{drop} or is overshadowed by a magnetic order.

Finally, we address the freezing out of $\kappa_{\mathrm{spinon}}/T$ below T_{drop}. The depleted κ_{spinon} signal can either indicate a spinon excitation gap or the loss of coupling between spinons and the phonon background [61], through which κ of an insulator is measured. Future work is required to clarify which of these two scenarios is valid (see [42]).

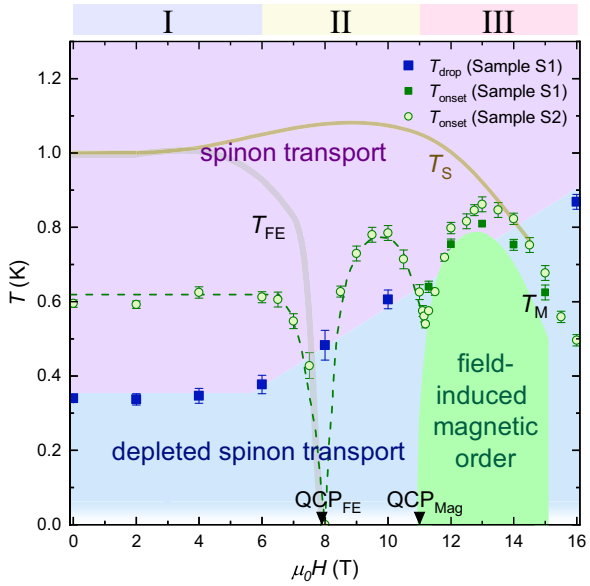

FIG. 3. Phase diagram of $PbCuTe_2O_6$ showing T_{onset} of samples S1 (green squares) and S2 (circles) as well as T_{drop} (sample S1) together with T_{FE}, T_{S} (dark yellow and gray lines), and T_{M} (top margin of light green area) as extracted from Ref. [57]. The ferroelectric $\mathrm{QCP_{FE}}$ at 7.9 T and magnetic $\mathrm{QCP_{mag}}$ at 11 T are reproduced from Ref. [57]. The evidence for a quantum spin liquid state (i.e., finite residual linear term a) is not affected by the ferroelectric or structural transitions; thus, it is ubiquitous in the parameter space colored in purple. The region below our experimental accessible range at $T \lesssim 50$ mK is left blank, except for the magnetically ordered phase.

To summarize, the high-quality low-T thermal conductivity of a 3D QSL candidate $PbCuTe_2O_6$ strongly suggests the existence of itinerant spinons, and thus of a spinon Fermi surface. The spinon heat transport is shown to be intrinsic and robust against disorder and field-induced phases. Our work thus highlights $PbCuTe_2O_6$ as a unique model system for QSL research.

We acknowledge fruitful discussions with Wolfram Brenig, Elena Hassinger, and Matthias Vojta. We thank Michael Lang, Bernd Wolf, Paul Eibisch, and Christian Thurn for ample discussions about our parallel going experiments and for sharing their thermodynamic results with us before publication. We further thank Tino Schreiner and Danny Baumann for technical assistance. This project has been supported by the Deutsche Forschungsgemeinschaft through the Sonderforschungsbereich SFB 1143. Furthermore, this project has received funding from the European Research Council under the European Union's Horizon 2020 research and innovation program (Grant Agreement No. 647276—MARS—ERC-2014-CoG).

*c.hess@uni-wuppertal.de

[1] L. Balents, Spin liquids in frustrated magnets, Nature (London) **464**, 199 (2010).

[2] L. Savary and L. Balents, Quantum spin liquids: A review, Rep. Prog. Phys. **80**, 106502 (2017).

[3] Y. Zhou, K. Kanoda, and T. K. Ng, Quantum spin liquid states, Rev. Mod. Phys. **89**, 025003 (2017).

[4] C. Broholm, R. J. Cava, S. A. Kivelson, D. G. Nocera, M. R. Norman, and T. Senthil, Quantum spin liquids, Science **367**, eaay0668 (2020).

[5] X.-G. Wen, Quantum orders and symmetric spin liquids, Phys. Rev. B **65**, 165113 (2002).

[6] X.-G. Wen, Choreographed entanglement dances: Topological states of quantum matter, Science **363**, eaal3099 (2019).

[7] P. W. Anderson, Resonating valence bonds: A new kind of insulator?, Mater. Res. Bull. **8**, 153 (1973).

[8] P. A. Lee, An end to the drought of quantum spin liquids, Science **321**, 1306 (2008).

[9] M. J. P. Gingras and P. A. McClarty, Quantum spin ice: A search for gapless quantum spin liquids in pyrochlore magnets, Rep. Prog. Phys. **77**, 056501 (2014).

[10] Y. Okamoto, M. Nohara, H. Aruga-Katori, and H. Takagi, Spin-liquid state in the $S = 1/2$ hyperkagome antiferromagnet $Na_4Ir_3O_8$, Phys. Rev. Lett. **99**, 137207 (2007).

[11] C. Balz, B. Lake, J. Reuther, H. Luetkens, R. Schonemann, T. Herrmannsdorfer, Y. Singh, A. T. M. N. Islam, E. M. Wheeler, J. A. Rodriguez-Rivera, T. Guidi, G. G. Simeoni, C. Baines, and H. Ryll, Physical realization of a quantum spin liquid based on a complex frustration mechanism, Nat. Phys. **12**, 942 (2016).

[12] K. W. Plumb, H. J. Changlani, A. Scheie, S. Zhang, J. W. Krizan, J. A. Rodriguez-Rivera, Y. Qiu, B. Winn, R. J. Cava, and C. L. Broholm, Continuum of quantum fluctuations in a three-dimensional $S = 1$ Heisenberg magnet, Nat. Phys. **15**, 54 (2019).

[13] B. Gao *et al.*, Experimental signatures of a three-dimensional quantum spin liquid in effective spin-1/2 $Ce_2Zr_2O_7$ pyrochlore, Nat. Phys. **15**, 1052 (2019).

[14] S.-S. Lee, P. A. Lee, and T. Senthil, Amperean pairing instability in the U(1) spin liquid state with Fermi surface and application to κ-$(BEDT\text{-}TTF)_2Cu_2(CN)_3$, Phys. Rev. Lett. **98**, 067006 (2007).

[15] M. Yamashita, T. Shibauchi, and Y. Matsuda, Thermal-transport studies of two-dimensional quantum spin liquids, Chem. Phys. Chem. **13**, 74 (2012).

[16] C. Hess, H. ElHaes, A. Waske, B. Büchner, C. Sekar, G. Krabbes, F. Heidrich-Meisner, and W. Brenig, Linear temperature dependence of the magnetic heat conductivity in $CaCu_2O_3$, Phys. Rev. Lett. **98**, 027201 (2007).

[17] B. Y. Pan, Y. Xu, J. M. Ni, S. Y. Zhou, X. C. Hong, X. Qiu, and S. Y. Li, Unambiguous experimental verification of linear-in-temperature spinon thermal conductivity in an antiferromagnetic Heisenberg chain, Phys. Rev. Lett. **129**, 167201 (2022).

[18] N. Hlubek, P. Ribeiro, R. Saint-Martin, A. Revcolevschi, G. Roth, G. Behr, B. Büchner, and C. Hess, Ballistic heat transport of quantum spin excitations as seen in $SrCuO_2$, Phys. Rev. B **81**, 020405(R) (2010).

[19] M. Yamashita, N. Nakata, Y. Senshu, M. Nagata, H. M. Yamamoto, R. Kato, T. Shibauchi, and Y. Matsuda, Highly mobile gapless excitations in a two-dimensional candidate quantum spin liquid, Science **328**, 1246 (2010).

[20] J. M. Ni, B. L. Pan, B. Q. Song, Y. Y. Huang, J. Y. Zeng, Y. J. Yu, E. J. Cheng, L. S. Wang, D. Z. Dai, R. Kato, and S. Y. Li, Thermal conductivity of the quantum spin liquid candidate $EtMe_3Sb[Pd(dmit)_2]_2$: No evidence of mobile gapless excitations, Phys. Rev. Lett. **123**, 247204 (2019).

[21] P. Bourgeois-Hope, F. Laliberte, E. Lefrancois, G. Grissonnanche, S. Rene de Cotret, R. Gordon, S. Kitou, H. Sawa, H. Cui, R. Kato, L. Taillefer, and N. Doiron-Leyraud, Absence of magnetic thermal conductivity in the quantumspin liquid candidate $EtMe_3Sb[Pd(dmit)_2]_2$, Phys. Rev. X **9**, 041051 (2019).

[22] Y. J. Yu, Y. Xu, L. P. He, M. Kratochvilova, Y. Y. Huang, J. M. Ni, L. Wang, S.-W. Cheong, J.-G. Park, and S. Y. Li, Heat transport study of the spin liquid candidate 1T-TaS_2, Phys. Rev. B **96**, 081111(R) (2017).

[23] H. Murayama, Y. Sato, T. Taniguchi, R. Kurihara, X. Z. Xing, W. Huang, S. Kasahara, Y. Kasahara, I. Kimchi, M. Yoshida, Y. Iwasa, Y. Mizukami, T. Shibauchi, M. Konczykowski, and Y. Matsuda, Effect of quenched disorder on the quantum spin liquid state of the triangular-lattice antiferromagnet 1T-TaS_2, Phys. Rev. Res. **2**, 013099 (2020).

[24] N. Li, Q. Huang, X. Y. Yue, W. J. Chu, Q. Chen, E. S. Choi, X. Zhao, H. D. Zhou, and X. F. Sun, Possible itinerant excitations and quantum spin state transitions in the effective spin-1/2 triangular-lattice antiferromagnet $Na_2BaCo(PO_4)_2$, Nat. Commun. **11**, 4216 (2020).

[25] X. Rao *et al.*, Survival of itinerant excitations and quantum spin state transitions in $YbMgGaO_4$ with chemical disorder, Nat. Commun. **12**, 4949 (2021).

[26] S. Guang, N. Li, R. L. Luo, Q. Huang, Y. Wang, X. Yue, K. Xia, Q. Li, X. Zhao, G. Chen, H. Zhou, and X. Sun, Thermal transport of fractionalized antiferromagnetic and field-induced states in the Kitaev material $Na_2Co_2TeO_6$, Phys. Rev. B **107**, 184423 (2023).

[27] X. C. Hong, M. Gillig, W. L. Yao, L. Janssen, V. Kocsis, S. Gass, Y. Li, A. U. B. Wolter, B. Buchner, and C. Hess, Phonon thermal transport shaped by strong spin-phonon scattering in a Kitaev material $Na_2Co_2TeO_6$, arXiv:2306.16963.

[28] M. Yamashita, Y. Sato, T. Tominaga, Y. Kasahara, S. Kasahara, H. Cui, R. Kato, T. Shibauchi, and Y. Matsuda, Presence and absence of itinerant gapless excitations in the quantum spin liquid candidate $EtMe_3Sb[Pd(dmit)_2]_2$, Phys. Rev. B **101**, 140407(R) (2020).

[29] Y. Y. Huang, Y. Xu, L. Wang, C. C. Zhao, C. P. Tu, J. M. Ni, L. S. Wang, B. L. Pan, Y. Fu, Z. Hao, C. Liu, J.-W. Mei, and S. Y. Li, Heat transport in herbertsmithite: Can a quantum spin liquid survive disorder?, Phys. Rev. Lett. **127**, 267202 (2021).

[30] Z. Zhu, P. A. Maksimov, S. R. White, and A. L. Chernyshev, Disorder-induced mimicry of a spin liquid in $YbMgGaO_4$, Phys. Rev. Lett. **119**, 157201 (2017).

[31] J. R. Chamorro, T. M. McQueen, and T. T. Tran, Chemistry of quantum spin liquids, Chem. Rev. **121**, 2898 (2021).

[32] Z. Ma, Z.-Y. Dong, S. Wu, Y. Zhu, S. Bao, Z. Cai, W. Wang, Y. Shangguan, J. Wang, K. Ran, D. Yu, G. Deng, R. A. Mole, H.-F. Li, S.-L. Yu, J.-X. Li, and J. S. Wen,

Disorder-induced spin-liquid-like behavior in kagome-lattice compounds, Phys. Rev. B **102**, 224415 (2020).
[33] D. S. Inosov, Quantum magnetism in minerals, Adv. Phys. **67**, 149 (2018).
[34] B. Koteswararao, R. Kumar, P. Khuntia, S. Bhowal, S. K. Panda, M. R. Rahman, A. V. Mahajan, I. Dasgupta, M. Baenitz, K. H. Kim, and F. C. Chou, Magnetic properties and heat capacity of the three-dimensional frustrated $S = 1/2$ antiferromagnet $PbCuTe_2O_6$, Phys. Rev. B **90**, 035141 (2014).
[35] S. Chillal, Y. Iqbal, H. O. Jeschke, J. A. Rodriguez-Rivera, R. Bewley, P. Manuel, D. Khalyavin, P. Steffens, R. Thomale, A. T. M. N. Islam, J. Reuther, and B. Lake, Evidence for a three-dimensional quantum spin liquid in $PbCuTe_2O_6$, Nat. Commun. **11**, 2348 (2020).
[36] Y. Zhou, P. A. Lee, T.-K. Ng, and F.-C. Zhang, $Na_4Ir_3O_8$ as a 3D spin liquid with fermionic spinons, Phys. Rev. Lett. **101**, 197201 (2008).
[37] E. J. Bergholtz, A. M. Lauchli, and R. Moessner, Symmetry breaking on the three-dimensional hyperkagome lattice of $Na_4Ir_3O_8$, Phys. Rev. Lett. **105**, 237202 (2010).
[38] P. Khuntia, F. Bert, P. Mendels, B. Koteswararao, A. V. Mahajan, M. Baenitz, F. C. Chou, C. Baines, A. Amato, and Y. Furukawa, Spin liquid state in the 3D frustrated antiferromagnet $PbCuTe_2O_6$: NMR and muon spin relaxation studies, Phys. Rev. Lett. **116**, 107203 (2016).
[39] A. R. N. Hanna, A. T. M. N. Islam, R. Feyerherm, K. Siemensmeyer, K. Karmakar, S. Chillal, and B. Lake, Crystal growth, characterization, and phase transition of $PbCuTe_2O_6$, Phys. Rev. Mater. **5**, 113401 (2021).
[40] C. Thurn, P. Eibisch, A. Ata, M. Winkler, P. Lunkenheimer, I. Kezsmarki, U. Tutsch, Y. Saito, S. Hartmann, J. Zimmermann, A. R. N. Hanna, A. T. M. N. Islam, S. Chillal, B. Lake, B. Wolf, and M. Lang, Spin liquid and ferroelectricity close to a quantum critical point in $PbCuTe_2O_6$, npj Quantum Mater. **6**, 95 (2021).
[41] P. D. Thacher, Effect of boundaries and isotopes on the thermal conductivity of LiF, Phys. Rev. **156**, 975 (1967).
[42] See Supplemental Material at http://link.aps.org/supplemental/10.1103/PhysRevLett.131.256701 for experimental details, additional data and analysis, estimation of the spinon mean free path, and more discussions on specific features, which includes Refs. [43–52].
[43] G. G. Ihas, L. Frederick, and J. P. McFarland, Low temperature thermometry in high magnetic fields, J. Low Temp. Phys. **113**, 963 (1998).
[44] R. Hentrich, A. U. B. Wolter, X. Zotos, W. Brenig, D. Nowak, A. Isaeva, T. Doert, A. Banerjee, P. Lampen-Kelley, D. G. Mandrus, S. E. Nagler, J. Sears, Y.-J. Kim, B. Buchner, and C. Hess, Unusual phonon heat transport in α-$RuCl_3$: Strong spin-phonon scattering and field-induced spin gap, Phys. Rev. Lett. **120**, 117204 (2018).
[45] J. Callaway, Low-temperature lattice thermal conductivity, Phys. Rev. **122**, 787 (1961).
[46] J. Callaway, Model for lattice thermal conductivity at low temperatures, Phys. Rev. **113**, 1046 (1959).
[47] S. Y. Li, J.-B. Bonnemaison, A. Payeur, P. Fournier, C. H. Wang, X. H. Chen, and L. Taillefer, Low-temperature phonon thermal conductivity of single-crystalline Nd_2CuO_4: Effects of sample size and surface roughness, Phys. Rev. B **77**, 134501 (2008).
[48] Q. Barthelemy, E. Lefrancois, J. Baglo, P. Bourgeois-Hope, D. Chatterjee, P. Lefloic, M. Velazquez, V. Baledent, B. Bernu, N. Doiron-Leyraud, F. Bert, P. Mendels, and L. Taillefer, Heat conduction in herbertsmithite: Field dependence at the onset of the quantum spin liquid regime, Phys. Rev. B **107**, 054434 (2023).
[49] C. P. Tu, D. Z. Dai, X. Zhang, C. C. Zhao, X. B. Jin, B. Gao, T. Chen, P. C. Dai, and S. Y. Li, Evidence for gapless quantum spin liquid in a honeycomb lattice, arXiv:2212.07322.
[50] L. E. Chern and Y. B. Kim, Theoretical study of quantum spin liquids in $S = 1/2$ hyper-hyperkagome magnets: Classification, heat capacity, and dynamical spin structure factor, Phys. Rev. B **104**, 094413 (2021).
[51] D. Watanabe, K. Sugii, M. Shimozawa, Y. Suzuki, T. Yajima, H. Ishikawa, Z. Hiroi, T. Shibauchi, Y. Matsuda, and M. Yamashita, Emergence of nontrivial magnetic excitations in a spin-liquid state of kagome volborthite, Proc. Natl. Acad. Sci. U.S.A. **113**, 8653 (2016).
[52] M. Fu, T. Imai, T.-H. Han, and Y. S. Lee, Evidence for a gapped spin-liquid ground state in a kagome Heisenberg antiferromagnet, Science **350**, 655 (2015).
[53] R. Berman, *Thermal Conduction in Solids* (Clarendon Press, Oxford, 1976).
[54] Attributing bT^3 to κ_{ph} is endorsed by the very good agreement of the fitted κ_{ph} and the extrapolated κ_{ph} (Fig. 1) from the high-temperature κ data as an independent evaluation, which depends on the dominance of canonical κ_{ph} in $PbCuTe_2O_6$ at high enough temperatures [42].
[55] M. Gillig, X. C. Hong, P. Sakrikar, G. Bastien, A. U. B. Wolter, L. Heinze, S. Nishimoto, B. Buchner, and C. Hess, Thermal transport of the frustrated spin-chain mineral linarite: Magnetic heat transport and strong spin-phonon scattering, Phys. Rev. B **104**, 235129 (2021).
[56] X. C. Hong, M. Behnami, L. Yuan, B. Li, W. Brenig, B. Buchner, Y. S. Li, and C. Hess, Heat transport of the kagome Heisenberg quantum spin liquid candidate $YCu_3(OH)_{6.5}Br_{2.5}$: Localized magnetic excitations and a putative spin gap, Phys. Rev. B **106**, L220406 (2022).
[57] P. Eibisch, C. Thurn, A. Ata, Y. Saito, S. Hartmann, U. Tutsch, B. Wolf, A. T. M. N. Islam, S. Chillal, A. R. N. Hanna, B. Lake, and M. Lang, Field-induced effects in the spin liquid candidate $PbCuTe_2O_6$, Phys. Rev. B **107**, 235133 (2023).
[58] We point out that a linear contribution is not observed in the heat capacity measurement in the sub-kelvin regime [38–40], presumably because of the dominance of the entropy associated with the ferroelectric transition.
[59] F. Forte, J. van den Brink, and M. Cuoco, Evolution of spinon Fermi surface and magnetic response of hyperkagome spin liquids, Phys. Rev. B **88**, 144422 (2013).
[60] Y. Shen, Y.-D. Li, H. C. Walker, P. Steffens, M. Boehm, X. Zhang, S. Shen, H. Wo, G. Chen, and J. Zhao, Fractionalized excitations in the partially magnetized spin liquid candidate $YbMgGaO_4$, Nat. Commun. **9**, 4138 (2018).
[61] M. F. Smith, J. Paglione, M. B. Walker, and L. Taillefer, Origin of anomalous low-temperature downturns in the thermal conductivity of cuprates, Phys. Rev. B **71**, 014506 (2005).